Large Eddy Simulation of a polydisperse, evaporating spray jet with a presumed function method of moments

P. Dems*[1], J.N.E. Carneiro[2], W. Polifke[1]
[1]Lehrstuhl für Thermodynamik, TU München, Germany
[2]Instituto SINTEF do Brasil, Rio de Janeiro, Brazil
dems@td.mw.tum.de, joao.carneiro@sintefbrasil.org.br and polifke@td.mw.tum.de

Abstract

A polydisperse Eulerian-Eulerian two-phase model has been used to simulate evaporation of acetone droplets dispersed in an air jet. The presumed function method of moments model considers the polydispersity of the spray in terms of droplet diameter by transporting low order moments of the particle size distribution function. This approach takes into account the dependency on the droplet diameter of particle motion, evaporation rates and phase interaction forces, e.g. drag. Unknown moments, e.g. higher order moments which are not transported but needed for closure, are calculated assuming a functional form of the number density function. The development of the model including validity of moment sets and formulations for Reynolds-Averaged Navier-Stokes and Large Eddy Simulations as well as the application to several configurations of cold particle-laden and bubbly flows have been shown in previous publications.
The objective of the work presented in this study was the formulation and application of the model for non-isothermal flows. The model is validated against data obtained from evaporating spray measurements.

Introduction

Detailed understanding, further development and optimisation of industrial spray applications, as e.g. diesel engines, aircraft gas turbines or process industry, rely more and more on the application of advanced CFD tools to predict the multi-phase flow behaviour and describe a variety of flow phenomena in a detailed manner which are often difficult or even impossible to separate in experiments. Compared to the Euler-Lagrange methodology, which allows to simulate monodispersed as well as polydispersed fluid-particle systems without significant differences in the modelling approach, Euler-Euler formulations require extensive modelling to capture polydispersity, i.e. effects dependent on the dispersed particle size (drag, lift, aerodymanic and thermal response times, etc.) or effects dependent on any other particle property, which may differ from particle to particle. Despite the challenges coming along with the Eulerian-Eulerian formulation, increasing research has been undertaken in the last decade to enforce the accuracy, performance and stability of Euler-Euler two-phase simulation tools. A main reason for this is the applicability of Euler-Euler simulation tools for large scale industrial applications whereas in Euler-Lagrange simulations the computational effort scales inversely with the number of particles needed to ensure a proper representation of the flow.

Several types of moment methods, which describe the development of e.g. the size distribution function of particles dispersed in a continuous fluid by its moments, were developed. Applications as e.g. spray combustion require, besides the description of the spray kinetics, the incorporation of heat and mass transfer and combustion modelling. A comprehensive model including polydisperse evaporation of droplets was derived by Beck and Watkins [1, 2, 3] and applied e.g. in Jager and Kok [4] or Dhuchakallaya and Watkins[5] for RANS simulation of spray combustion. Eulerian-Eulerian evaporating spray LES simulations have been reported e.g. by Masi et al. [6, 7], Boileau et al. [8] and Chaisemartin et al. [9]. Kah et al. [10] and Massot et al. [11] contributed to fundamental theoretical work on accurate moment transport in cold and evaporating cases, respectively. Considering the fact that Eulerian-Eulerian LES of polydisperse, evaporating and reactive sprays using moment methods is a demanding task regarding development of robust models and numerical methods, as well as stable and reliable simulations of practical configurations, it remains an open field of research in many aspects.

A detailed description of the presumed function method of moments used in this work to capture polydispersity in particle-laden flows can be found elsewhere (Carneiro et al.[12, 13]). Therefore only a brief overview of the basic model equations is given in the next section, followed by the extension to non-isothermal flows. Derivation of the evaporation source terms and the coupling of the compressible gas phase with the particle phase are shown. The evaporation rate is determined using a modified film model due to the Stefan flow and the correction of the

*Corresponding author: dems@td.mw.tum.de

Sherwood and Nusselt numbers by the Frossling correlation. To obtain source terms for the moment transport equations, the formulation is integrated over the diameter spectrum. In the filtered LES equations, these source terms were determined by using the averaged flow properties. The model is then validated against the experimental measurements made at the spray burner as described e.g. in [14, 15, 16]. This configuration has also been used several times for the validation of Eulerian-Lagrangian evaporating spray simulations (Jones et al. [17], Bini and Jones [18], De and Lakshmisha [19], Chrigui et al. [20]).

Model Formulation

Dispersed Phase Equations

The basic ideas of the presumed function method of moments as proposed by Carneiro et al. [12, 13] are briefly recapitulated to give an understanding of the method used in this paper. It provides the background to embed the equations and source terms arising due to the incorporation of spray evaporation, which is the purpose of the present work. The basic principle of moment methods is to solve transport equations for low order moments of the probability density function of interest. In dispersed phase flows, polydispersity is often referred to the effect of the particle size on particle dynamics and phase interaction forces. Therefore, transport equations for the first low order moments of the particle size distribution function f(D) are usually solved.

A moment of k-th order in terms of the particle diameter D as internal variable is defined as

$$M^{(k)} \equiv \int_0^\infty D^k f(D)\, dD \; . \tag{1}$$

A transport equation for the moments can be derived by integrating the multi-fluid dispersed phase mass conservation equation over the diameter spectrum. For constant disperse phase density ρ_d, this yields

$$\frac{\partial M^{(k)}}{\partial t} + \nabla \cdot \left(M^{(k)} \mathbf{u}^{(k)} \right) = \frac{1}{\rho_d} \Gamma_{M^{(k)}} \; . \tag{2}$$

$\Gamma_{M^{(k)}}$ is the source/sink term due to mass transfer from one phase to another, e.g. evaporation. Each moment is advected with its respective moment transport velocity

$$\mathbf{u}^{(k)} \equiv \frac{1}{M^{(k)}} \int_0^\infty \mathbf{u}(D) D^k f(D)\, dD \; . \tag{3}$$

Assuming that all particles have the same velocity $\mathbf{u}_p$, it results $\mathbf{u}^{(k)} = \mathbf{u}_p$. Otherwise $\mathbf{u}^{(k)} \neq \mathbf{u}_p$, which is in general the case. This ensures to capture the effect that particles with different sizes relax differently fast towards the continuous phase velocity $\mathbf{u}_c$. With the same procedure, the dispersed phase momentum conservation equation can be derived. Considering pressure and laminar shear dispensable in a dilute particulate phase, neglecting gravity and assuming that particles with the same diameter have locally the same velocity, it reads

$$\frac{\partial \left(M^{(3)} \mathbf{u}^{(3)} \right)}{\partial t} + \nabla \cdot \left(M^{(3)} \mathbf{u}^{(3)} \mathbf{u}^{(3)} \right) = \frac{1}{\rho_d} \left[- \int_0^\infty \mathbf{M}_{\text{Drag}}\, dD + \int_0^\infty \Gamma(D) \mathbf{u}(D) D^3 f(D)\, dD \right] \; . \tag{4}$$

where the first term on the right hand side represents the phase interaction forces represented by drag, lift, etc. (here only drag is considered) and the second term is the momentum exchange between phases due to mass transfer from one phase to another. To avoid solving a moment flux transport equation for each moment transport velocity, Carneiro et al. [12] derived an integrated version of the relaxation approach proposed by Bollweg et al. [21], which determines minor particle size velocities from a linear interpolation between a reference particle velocity and the continuous phase velocity. This approach used the idea of the "Equilibrium Eulerian Method" originally introduced by Ferry and Balachandar [22, 23]. With that, using the mass averaged dispersed phase velocity $\mathbf{u}^{(3)}$ as reference velocity, unknown moment transport velocities can be determined by

$$\mathbf{u}^{(k)} \approx \mathbf{u}_c + \frac{\tau^{(k)}}{\tau^{(3)}} \left(\mathbf{u}^{(3)} - \mathbf{u}_c \right) \quad \text{with } \tau^{(k)} \propto \frac{M^{(k+2)}}{M^{(k)}} \; . \tag{5}$$

The kinetic particle relaxation times in their integral form $\tau^{(k)}$, i.e. averaged over the diameter spectrum, depend on a moment of the same order k, but also on a moment of order k+2. This closure problem can be resolved by assuming a functional form of the particle size distribution function. Here we use the Gamma distribution, which can be reconstructed from three consecutive moments. Due to modelling reasons (details later on), we use the

moments $M^{(1)}$-$M^{(3)}$ as *prognostic* moments, i.e. transported and therefore known moments, to reconstruct the Gamma distribution. The *diagnostic* moments, e.g. $M^{(0)}$, which are needed for closure of the source terms, can be calculated from the reconstructed Gamma distribution. Each moment set must fulfil a set of constraints to be able to reconstruct a function (*realizable* or valid moment set). The so called Hankel-Hadamard determinants are a necessary condition for a valid moment set. It is not guaranteed that during the simulation a valid moment set is given in each computational cell, even if the initial and boundary moment sets are valid. Therefore, a mechanism must apply to adjust moments to ensure valid moment set throughout the computational domain. Further details on these conditions and those additionally arising due to the use of the Gamma distribution are outlined in [24], where LES of a particle laden swirling jet has been performed. The same procedure to obtain valid moment sets as described therein is used here.

The following formulation for the drag force momentum source term has been used in the moment flux transport equation for the third moment

$$\int_0^\infty \mathbf{M}_{\text{Drag}}\, dD = 18\mu_c \Bigg[\underbrace{M^{(1)}\left(\mathbf{u}^{(1)} - \mathbf{u}_c\right)}_{\text{analytically (Stokes)}} + \underbrace{0.15\left(\frac{|\mathbf{u}^{(1)} - \mathbf{u}_c|}{\nu_c}\right)^{0.687} M^{(1.687)}\left(\mathbf{u}^{(1.687)} - \mathbf{u}_c\right)}_{\text{approximated (Schiller and Naumann extension)}} \Bigg] . \quad (6)$$

The detailed derivation and the approximations made are outlined by [24].

Finally the equation for the particle phase sensible enthalpy h_d including the approximations shown later on for the mass vaporisation rate reads (with Δh_v latent heat, Nu Nusselt number and k_c thermal conductivity)

$$\frac{\partial \rho_d M^{(3)} h_d}{\partial t} + \nabla \cdot \left(\rho_d M^{(3)} \mathbf{u}^{(3)} h_d\right) = \Gamma_{M^{(3)}}\left(h_d + \Delta h_v\right) + 6\,\text{Nu}\, k_c M^{(1)}\left(T_c - T_d\right) . \quad (7)$$

All particles are assumed for simplicity to have locally the same temperature, i.e. $T(D) = T_d$. Watkins [26] has relaxed this hypothesis, formulating expressions for averaged temperatures $T^{(k)}$.

Gas Phase Equations

The transport equations for a compressible gas phase, considering small particle loadings will be considered below - in a similar framework as employed by [8]. The gas phase continuity and vapour mass fraction equation are given by

$$\frac{\partial \rho_c}{\partial t} + \nabla \cdot (\rho_c \mathbf{u}_c) = -\frac{\pi}{6}\int_0^\infty \Gamma(D) D^3 f(D)\, dD , \quad (8)$$

$$\frac{\partial \rho_c Y_{v,\infty}}{\partial t} + \nabla \cdot (\rho_c Y_{v,\infty} \mathbf{u}_c) - \nabla \cdot (\mu_{c,\text{eff}} \nabla Y_{v,\infty}) = -\frac{\pi}{6}\int_0^\infty \Gamma(D) D^3 f(D)\, dD , \quad (9)$$

where $Y_{v,\infty}$ is the vapor mass fraction, and the momentum balance equation is given by

$$\frac{\partial \rho_c \mathbf{u}_c}{\partial t} + \nabla \cdot (\rho_c \mathbf{u}_c \mathbf{u}_c) = -\nabla p + \nabla \cdot \boldsymbol{\tau}_c + \frac{\pi}{6}\int_0^\infty \mathbf{M}_{\text{Drag}}\, dD - \frac{\pi}{6}\int_0^\infty \Gamma(D)\mathbf{u}(D) D^3 f(D)\, dD + \rho \mathbf{g} , \quad (10)$$

with the mass and momentum source terms inverse in sign compared to the dispersed phase equations. The subscript c referres to the continuous phase properties, which are a mixture of air and acetone vapour in the present case. The equation for the sensible enthalpy h_c of the continuous phase, i.e. the air-vapour mixture, reads

$$\frac{\partial \rho_c h_c}{\partial t} + \nabla \cdot (\rho_c \mathbf{u}_c h_c) - \nabla \cdot (\mu_{c,\text{eff}} \nabla T_c) = -\frac{dp}{dt} - \frac{\pi}{6}\Gamma_{M^{(3)}} c_{p,v} T_d + \pi\,\text{Nu}\, k_c M^{(1)}\left(T_d - T_c\right) . \quad (11)$$

Since the gas temperature variation is small (compared to e.g. combustion simulations), air-vapour mixture viscosity μ_c and vapour heat capacity $c_{p,v}$ are assumed to be constant. The gas phase density ρ_c is given by the ideal gas law, given by $\rho_c = p/(\text{R}_{\text{mix}} T_c)$ with $\text{R}_{\text{mix}} = \text{R}_{\text{air}}(1 - Y_{v,\infty}) + \text{R}_v Y_{v,\infty}$.

Evaporation Source Terms

The determination of the mass exchange rate follows the approach of Abramzon and Sirignano [25], which is often used in Eulerian spray calculations. The evaporated mass flow rate for a single particle with diameter D including Stefan flux and forced convection can be determined by

$$\dot{m} = \pi \rho_c \mathcal{D} D \, \mathrm{Sh}^* \, \ln(1 + \mathrm{B_M}) \, , \tag{12}$$

where the Sherwood number $\mathrm{Sh}^* = 2 + 0.552\,\mathrm{Re}^{1/2}\mathrm{Sc}^{1/3}$ contains the enhanced vaporisation rate due to forced convection (Frossling correlation), $\mathcal{D}$ is the diffusion coefficient and Sc the Schmid number. $\mathrm{B_M}$ is the Spalding mass transfer number

$$\mathrm{B_M} = \frac{Y_{v,s} - Y_{v,\infty}}{1 - Y_{v,s}} \qquad \text{with } Y_{v,s} = \left[1 + \frac{W_C}{W_F}\left(\frac{p}{p_{F,s}} - 1\right)\right]^{-1} . \tag{13}$$

$Y_{v,s}$ is the vapor mass fraction at the droplet surface and sufficiently far away from the droplet ($Y_{v,\infty}$), where W_C and W_F are the molar mass of the continuous fluid and the droplets, respectively. The Clausius-Clayperon relation is used to determine the surface vapour pressure $p_{F,s}$. The mass vaporisation rate $\dot{m}$ can be integrated over the diameter spectrum, yielding:

$$\Gamma_{M^{(3)}} = -6\rho_c \mathcal{D} \ln(1 + \mathrm{B_M}) \left(2M^{(1)} + 0.552 \int_0^\infty \left(\frac{|\mathbf{u}(D) - \mathbf{u}_c|}{\nu_c} \right)^{0.5} D^{1.5} f(D)\, dD \; \mathrm{Sc}^{1/3} \right) . \tag{14}$$

To obtain a simple analytical solution, we substitute $\mathbf{u}(D)$ with an averaged moment transport velocity to resolve the dependency of the remaining integral on the particle velocity. However, it is not obvious which order of moment transport velocity introduces the least deviation to the exact solution. Initially, $\mathbf{u}(D) = \mathbf{u}^{(3)}$ was used by Carneiro et al. [12], in the present paper we use an approximation dependent on the order of the moments involved (the equation is showing the general source term found for a moment of order k):

$$\Gamma_{M^{(k)}} = -2k\rho_c \mathcal{D} \ln(1 + \mathrm{B_M}) \left(2M^{(k-2)} + 0.552 \left(\frac{|\mathbf{u}^{(k-1.5)} - \mathbf{u}_c|}{\nu_c} \right)^{0.5} M^{(k-1.5)} \mathrm{Sc}^{1/3} \right) . \tag{15}$$

It is obvious, that a problem arises using this formulation as source term for the zeroth moment transport equation, since it gives $\Gamma_{M^{(0)}} = 0$. A robust framework for the evaluation of the droplets disappearance rate is presented by Massot et al. [11]. However, for simplicity, in the present work the set $M^{(1)} - M^{(3)}$ is solved for, where all source terms are defined and which is sufficient to reconstruct the Gamma distribution. On the one hand, the choice of $M^{(1)}$ to $M^{(3)}$ conserves important global properties of the distribution such as total surface area and particle mass. On the other hand, the particle number density $M^{(0)}$ might also be an important property in evaporation calculations, where it is not a conserved scalar anymore.

The momentum source term due to mass transfer $\Gamma_{M^{(3)}}$ (needed for closure of Eqn.4 and Eqn.10) is obtained in a similar manner

$$\begin{aligned} \Gamma_{M^{(3)}} &= \int_0^\infty \Gamma(D)\mathbf{u}(D) D^3 f(D)\, dD \\ &= -6\rho_c \mathcal{D} \ln(1 + \mathrm{B_M}) \left(2M^{(1)}\mathbf{u}^{(1)} + 0.552 \left(\frac{|\mathbf{u}^{(1.5)} - \mathbf{u}_c|}{\nu_c} \right)^{0.5} \mathbf{u}^{(1.5)} M^{(1.5)} \mathrm{Sc}^{1/3} \right) . \end{aligned} \tag{16}$$

LES Filtering and Numerical Method

In LES the smallest structures of the gas and particle flow are expected to be smaller than the cell width. Therefore, a filtering procedure is needed. Filtering in LES can be defined by the convolution of a given function with a filtering kernel ("Top-Hat", Gaussian, etc.). Similar to Favre averaging, one can define a weighted filtering as follows:

$$\overline{M^{(k)}}\widetilde{\mathbf{u}^{(k)}} \equiv \int M^{(k)}(x)\mathbf{u}^{(k)}(x) F(x' - x) dx' \, , \tag{17}$$

where F is the filtering kernel function and the filtered (moment weighted) velocity $\widetilde{\mathbf{u}^{(k)}}$ is defined such that $\mathbf{u}^{(k)} = \widetilde{\mathbf{u}^{(k)}} + \mathbf{u}^{(k)\prime}$, with $\mathbf{u}^{(k)\prime}$ representing the unresolved velocity. We note that an analogous idea has been used

by [27], who defined the filtering by weighting with the particle number density. The integral moment and moment flux transport equations, describing the dispersed phase, are closed after the applied LES filtering by neglecting the dispersed phase subgrid-scale stress tensor and by replacing unfiltered by filtered variables in the drag term and evaporation source terms. A similar procedure applies to the dispersed phase enthalpy equation. This means that sub-grid scale effects of drag force and evaporation rates have not been considered so far. Favre-filtering (density based) is applied to the gas phase equations and sub-grid stresses are closed using the compressible, single phase Smagorinsky model.

The two-phase equation system and the moments model equations are implemented in OpenFOAM based on the solver `twoPhaseEulerFoam`. First attempts to sustain the original structure of the OpenFOAM solver `twoPhaseEulerFoam` by solving a pressure equation built with both the continuous and dispersed phase momentum equation, failed due to stability and convergence reasons. Instead, a serial solver structure is used, which first solves the incompressible equations of the dispersed phase, including the pressure-less and viscosity-free momentum equation, and afterwards solves the compressible equations of the continuous phase. Pressure, enthalpy and vapour mass fraction equation are solved sequentially within the PISO-loop. The computational cost for the polydisperse moments model is only 25% larger than that of the monodisperse solver, which is quite attractive.

Results and Discussion

Experimental and Numerical Setup

Experimental data on the particle size distributions are very important for the validation of polydisperse two-phase flow simulation models. Furthermore, inlet conditions are an important aspect. Since moment methods usually can not be used to describe the primary breakup of a spray, approximations must be made to set inlet conditions for cases where the spray is generated, e.g., by a pressurised or air-blast nozzle. Even more, the exact size distribution is often unknown in the near field of the nozzle. Therefore computational inlets have to be set sufficiently far downstream of the nozzle, where the primary breakup is completed. For this reason, experiments, where a definite distribution is already present at the actual inlet, are very advantageous. Such a case has been designed by a group at the University of Sydney (see e.g. [14], [15], [16]), using a generic spray burner. The spray is generated by an ultrasonic atomiser, which mixes afterwards with a coflow within a pipe. The configuration is designed to give a droplet size distribution approximately uniform across the pipe diameter. This droplet-laden air jet emanates the pipe with defined conditions and develops further downstream as a free jet surrounded by a slow, low-turbulence coflow. The numerical domain starts at this position where the two-phase jet emanates from the pipe and where detailed measurement data are available, which can be used as inlet condition. The pipe forming the droplet laden jet is surrounded by a coaxial pilot flame holder.

Measurements have been carried out for evaporating and combustion cases using several fuels and initial conditions. Here we use data of the measurement series SP3 of the acetone evaporating case. The inlet values for mass fluxes, mean particle sizes and moments of the size distribution are given in Table 1. 60% of the droplet mass is already vaporised when the droplet-laden jet emanates from the pipe. The moments are calculated from the experimental mean diameters via $D_{ab} = \left(M^{(a)}/M^{(b)}\right)^{1/(a-b)}$.

Table 1. Particle phase and gas phase conditions at the jet exit plane x=0 (inlet of simulation domain)

ρ_p	= 785 kg/m³	$M^{(0)}$	= 6.790609·10⁹ m^{-3}	Re	= 20700
$\dot{m}_c$	= 150 g/min	$M^{(1)}$	= 1.654046·10⁵ m^{-2}	ν_c	= 1.74 m²/s
$\dot{m}_v$	= 27.1 g/min	$M^{(2)}$	= 5.470325 m^{-1}	ρ_c	= 1.43 kg/m³
$\dot{m}_p$	= 17.9 g/min	$M^{(3)}$	= 2.26983·10^{-4}	T_c	= -5.5°C

Results

Simulations using the Sauter mean diameter D_{32} (i.e. locally monodisperse distributions - simply named "monodisperse" later on - where, however, spatial variations of the Sauter Mean Diameter are accounted for) as well as full polydisperse simulations using the moments model, as described above, have been carried out. In case of the monodisperse simulations, transport equations have been solved for the volume fraction of the droplets α and the

second moment $M^{(2)}$. With these properties the Sauter mean diameter can be calculated via $D_{32} = \pi\alpha/(6M^{(2)})$, on which the calculation of the drag force and the evaporation rate is based. The moment $M^{(2)}$ is transported with the same velocity $\mathbf{u}_d$ as the volume fraction as it is usually done in monodisperse two-phase simulations.

At the pipe exit, i.e. the inlet of the simulation domain, the spray is already pre-vaporised, indicated by a non-zero value for the vapour mass fraction at the inlet (Fig. 2). With progressing droplet evaporation, the particle mass (volume) decreases (Fig. 1) while the vapour amount increases (Fig. 2). The droplet mass is contained mainly in the large droplets which follow a rather straight line through the domain, whereas the vapour is convected with the turbulent gas phase velocity.

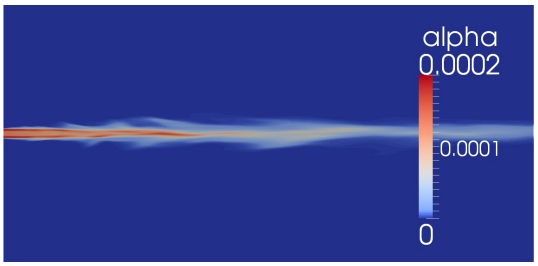

Figure 1. Instantaneous contours of the droplet volume fraction, polydispersed (rotated 90° clockwise)

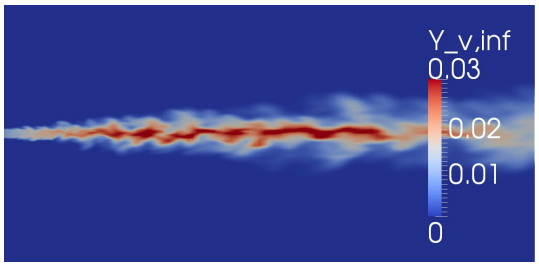

Figure 2. Instantaneous contours of the vapor mass fraction, polydispersed (rotated 90° clockwise)

The comparison of experimental and computed mean axial velocities (see first plot in Fig. 3), is satisfactory, but reveals deviations for both gas and dispersed phases. In both simulation types - monodispersed and polydispersed - the gas velocity is underpredicted. Apparently, different dispersed phase velocities in the monodispersed and polydispersed cases did not induce significant changes in the gas phase velocities. Therefore, the reason for the underpredictions is assigned to the inlet conditions for turbulence quantities, rather than momentum exchange through drag. Since particle size data are not available upstream of the jet exit plane, the mixing pipe is not included in the simulation domain. Instead, the turbulent pipe flow resulting from the upstream geometry and flow is modelled using a turbulence generator inlet boundary condition. However, the Reynolds stress tensor given as input is only estimated, leading to a rather moderate agreement of the gas velocity fluctuation components at the inlet. Significant improvement was observed further downstream, where the jet turbulence can develop (graphs are not shown).

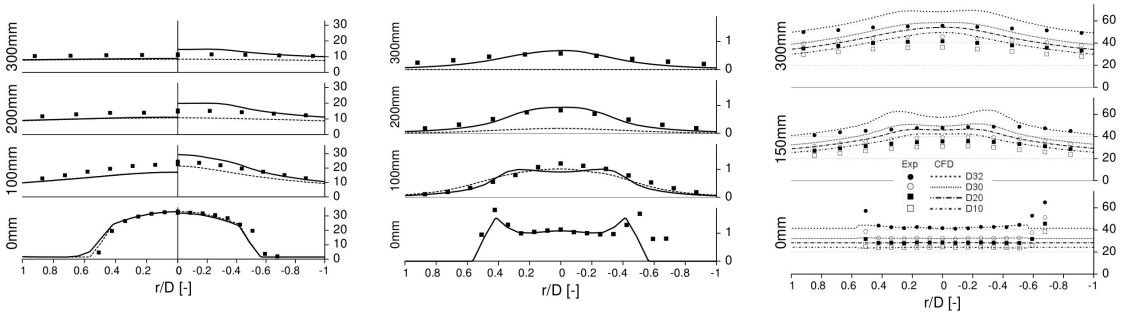

Figure 3. Left plot: **Axial mean velocity** (m/s) of gas (left part) and particles (right part). Centre plot: **Dispersed phase volume fraction** α (-) normalised with inlet value. Right plot: **Mean diameters** (m). Experiment (symbols) - monodispersed (dashed) - polydispersed (solid)

In the monodispersed case, particles seem to be decelerated too fast. This can be attributed to the fact that the drag force is evaluated using D_{32}, which is probably not the most appropriate measure to be used throughout the whole domain. In the polydispersed case, however, the particle velocity is overpredicted. Here, the strength of the drag force must be underpredicted by the moments model. The integrated drag term (Eqn.6) depends on two parameters, $M^{(1)}$ and $\mathbf{u}^{(1)}$ in the Stokes part and $M^{(1.687)}$ and $\mathbf{u}^{(1.687)}$ in the Schiller-Naumann part. Since experimental particle velocities are in general very close to the gas phase velocity, the moment transport velocities are assumed not to be responsible for the discrepancies in the polydispersed particle velocity. The prediction of the moment profiles remains as an important factor to be considered.

Moment profiles can be computed from the experimental particle diameter data, which allows the direct comparison with their numerical counterparts as shown in Fig. 4 and Fig. 3, center graph. Higher order moments $M^{(2)}$

and $M^{(3)}$ show good agreement with the experimental results, whereas the low order moments $M^{(0)}$ and $M^{(1)}$ predicted by the moments model are somewhat underpredicted in the region close to the centerline. Two reasons can be found. One the one hand, the moment transport velocities are controlled by the gas phase and the mass averaged particle velocity, and both presented some discrepancies from the experimental results. On the other hand, the sink terms due to evaporation have a significant impact. If the diameter sum ($M^{(1)}$) decreases to fast due to evaporation, we could see $M^{(1)}$ as the trigger for the overpredicted particle velocity, because it directly scales the drag force. Furthermore, the sink rates of $M^{(2)}$ and $M^{(1)}$ are directly proportional to $M^{(0)}$ and $M^{(-1)}$, respectively, which are determined by the Gamma distribution. Therefore, the decrease of $M^{(2)}$ and $M^{(1)}$ depends on the choice of the distribution function. Errors, potentially introduced by the determination of $M^{(0)}$ and $M^{(-1)}$ via the Gamma distribution, directly influence the higher order moments. At this point, we must dedicate the quantification of this effect to future investigation.

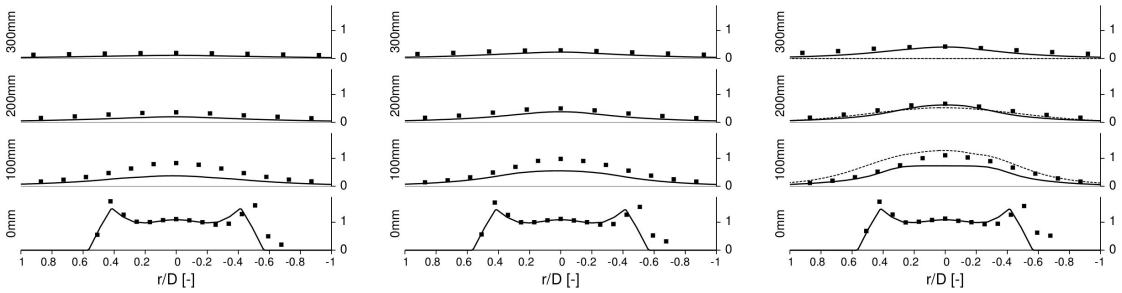

Figure 4. Moment $M^{(0)}$ (left), $M^{(1)}$ (center) and $M^{(2)}$ (right). Normalised with inlet values. Experiment (symbols) - polydisperse simulation (solid) - monodisperse simulation, only for $M^{(2)}$ (dashed)

Comparing monodisperse and polydisperse results, we see that the monodispersed particles with Sauter mean diameter are almost evaporated at x=200mm (Fig. 3 center graph). Contrary to this, the polydisperse model predicts the degree of mass loss in the dispersed phase much closer to the experimental findings.

For completeness, the mean diameters D_{10}, D_{20}, D_{30}, D_{32} are shown on the right in Fig. 3. They show the correct trend to increase downstream, but the growth is slightly overpredicted. This is in line with the information gained from the moment plots, where the zeroth and second moment deviate more from the experimental data than the third moment. This results - considering the definition of the mean diameters (see Section *Experiment and Numerical Setup*) - in the overprediction of the mean diameters.

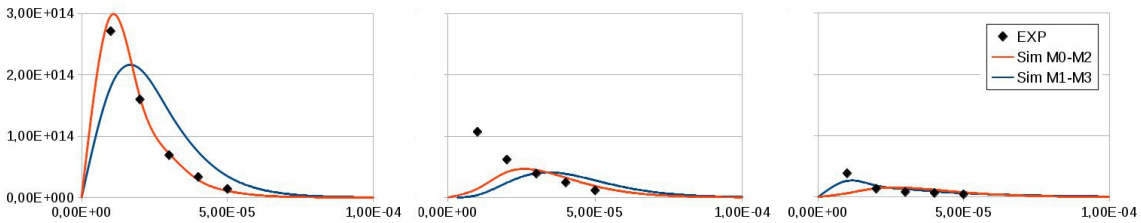

Figure 5. Droplet size distribution functions at centerline at 0mm (inlet, left), 150mm (center) and 300mm (right)

Finally, it is helpful to analyse the size distribution functions directly to estimate how the deviations in the moment values relate to the shape of the particle size distributions. Fig. 5 shows three number density distributions at different positions located at the centerline. Plotted are both, the Gamma distribution reconstructed from the three *prognostic*, i.e. transported, moments $M^{(1)}$ to $M^{(3)}$ and from the set $M^{(0)}$ to $M^{(2)}$. The choice of the type of reconstruction significantly changes the visual match of reconstructed and experimental size distribution functions, although the moments $M^{(1)}$ and $M^{(2)}$ are common in both cases. It is obvious from the visual analysis, that there is a lack of small droplets (especially at x=150mm), which is compensated by a larger amount of large droplets than observed in experiments. This is, however, not a drawback of the Gamma distribution shape, since it is able to represent positively skewed distributions very well, as it is the case of the initial distribution and at x=300mm.

Summary and Conclusions

A moments model, transporting the low order moments of the particle size distribution function with their respective moment transport velocities, has been applied to simulate acetone spray evaporation at room temperature. Predictions of moment profiles and mean diameters suggest that the evaporating mass rates compare reasonably well with experimental findings. Here, a significant improvement by using the polydisperse model compared to the "monodisperse" simulation (using the Sauter mean diameter) can be observed. Within the scope of the chosen setup including the Gamma distribution, the Uniform Temperature Model for droplet evaporation and the independence of droplet temperature on diameter, it has been shown that a quite reasonable overall agreement is obtained for size distributions and their low order moments. It was also observed that, large particles evaporates slower and small particles faster than in the experiment. Building upon the presented results, investigations on the impact of the mentioned assumptions is the subject of ongoing and future work.

Acknowledgements

The authors want to acknowledge the financial support given by ALSTOM (Germany) and the state of Bavaria in the framework of the research initiative KW21 II Project BY14GV.

References

[1] Beck, J. C. and Watkins, A. P. *J. of Computational Physics* 182:586-621 (2002).
[2] Beck, J. C. and Watkins, A. P. *Proc. R. Soc. Lond. A.* 459:1365-1394 (2003).
[3] Beck, J. C. and Watkins, A. P. *Int. J. of Heat and Fluid Flow* 24:242-259 (2003).
[4] de Jager, B. and Kok, J. B. W. *Appplied Thermal Engineering* 24:1481-1489 (2004).
[5] Dhuchakallaya, I. and Watkins, A. P. *Applied Thermal Engineering* 30:1215-1224 (2010).
[6] Masi, E., Bédat, B., Moreau, M. and Simonin, O. *Proc. of FEDSM2008* (2008).
[7] Masi, E., Simonin, O. and Bédat, B. *Flow Turbulence Combustion* 86:563-583 (2011).
[8] Boileau, M., Pascaud, S., Riber, E., Cuenot, B., Gicquel, L. Y. M., Poinsot, T. J. and Cazalens, M. *F*low Turbulence Combustion 80:291-321 (2008).
[9] de Chaisemartin, S., Fréret, L., Kah, D., Laurent, F., Fox, R. O., Reveillon, J. and Massot, M. *Proc. of the Summer Program, Center for Turbulence Research, Stanford* (2008).
[10] Kah, D., Laurent, F., Massot, M. and Jay, S. *Journal of Computational Physics* 231-2:394-422 (2012).
[11] Massot, M. Laurent, F., Kah, D. and de Chaisemartin, S. *SIAM Journal on Applied Mathematics* 70-8:3203-3234 (2010).
[12] Carneiro, J. N. E., Kaufmann, V. and Polifke, W. *Proceedings of COBEM, Gramado, Brazil* (2009).
[13] Carneiro, J. N. E., Dems, P., Kaufmann, V. and Polifke, W. *7th ICMF 2010, Tampa, FL* (2010).
[14] Chen, Y. C., Stårner, S. H., Masri, A. R. *Proc. of the Combustion Institute* 29:625-632 (2002).
[15] Stårner, S. H., Gounder, J., Masri, A. R. *Combustion and Flame* 143:420-432 (2005).
[16] Chen, Y. C., Stårner, S. H., Masri, A. R. *International Journal of Multiphase Flow* 32:389-412 (2006).
[17] Jones, W. P., Lyra, S., Marquis, A. J. *Int. Journal of Heat and Mass Transfer* 53:2491-2505 (2010).
[18] Bini, M., Jones, W. P. *Int. Journal of Heat and Fluid Flow* 30:471-480 (2009).
[19] De, S., Lakshmisha, K. N. *Int. Journal of Spray and Combustion Dynamics* 1-2:169-198 (2009).
[20] Chrigui, M. Sadiki, A., Gounder, J. and Masri, A. *Proc. of the ASME Turbo Expo* GT2011-46301 (2011).
[21] Bollweg, P., Kaufmann, A. and Polifke, W. *6th Int. Conference on Multiphase Flow, Leipzig, Germany* (2007).
[22] Ferry, J. and Balachandar, S. *Int. J. of Multiphase Flow* 27:1199-1226 (2001).
[23] Ferry, J. and Balachandar, S. *Powder Technology* 125:131-139 (2002).
[24] Dems, P., Carneiro, J. N. E. and Polifke, W. *Progress in Computational Fluid Dynamics* 12:92-102 (2012).
[25] Abramzon, B., Sirignano, W. A. *International Journal of Heat and Mass Transfer* 32-9:1605-1618 (1989).
[26] Watkins, A. P. *Int. J. of Heat and Fluid Flow* 28:388-406 (2007).
[27] Riber, E., Moreau, M., Simonin, O. and Cuenot, B. *Proceedings of FEDSM2006, ASME Joint U.S. - European Fluids Engineering Summer Meeting* (2006).